RESEARCH REPORT

VTT-R-00884-23

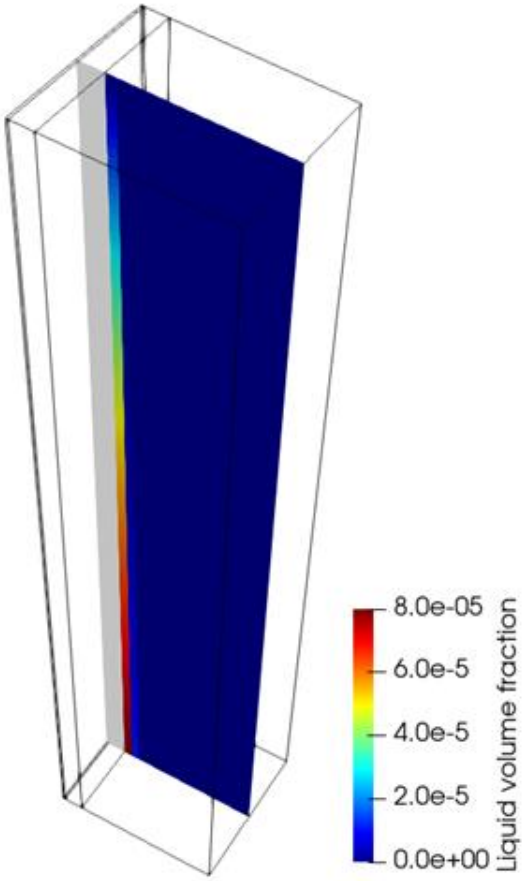

Validation of a surface condensation model for PWR containment analysis

Authors: Jouni Syrjänen, Ville Hovi

Confidentiality: VTT Public

Version: 31.12.2023

VTT

beyond the obvious

Report's title Validation of a surface condensation model for PWR containment analysis	
Customer, contact person, address Valtion Ydinjätehuoltorahasto Linda Kumpula (Työ- ja elinkeinoministeriö) PL 32, 00023 Valtioneuvosto	**Order reference** Dnro SAFER 16/2023
Project name CFD for Reactor Safety	**Project number/Short name** 136381 / SAFER2028_CeReSa_2023
Author(s) Jouni Syrjänen, Ville Hovi	**Pages** 18/
Keywords PWR, Containment, CFD	**Report identification code** VTT-R-00884-23

Summary

Validation calculations of a surface condensation model, developed and implemented in OpenFOAM CFD software at VTT as a part of a containment model, are conducted. The condensation model is based on multicomponent diffusion. The model was validated against experiments conducted with the CONAN test facility. The test device contains a channel with a cooled plate where condensation from mixture of steam and air flowing by takes place.

Effects of grid density, inflow velocity and turbulence damping were studied. Validation simulations using various inflow velocities and grid densities with and without turbulence damping were performed.

The agreement of simulated and measured condensation rates is best at low inflow velocities, with cell size averaged discrepancy to measured values below 4% at 1.5 m/s. The average discrepancy then increases with increasing inflow velocity up to about 21% at 3.5 m/s.

Regarding cell size, the best inflow velocity averaged agreement is obtained with 20 mm cell size with 9% discrepancy to measured value. The average discrepancy grows to 14% with 5 mm cell size, but there is no common trend among inflow velocity averaged cell sizes in this range. 20 mm cell size is reasonable to be used in practical containment simulations.

Including turbulence damping in the modelling decreases the condensation rates to some degree. The average discrepancy between simulated and measured condensation rates increases about 1-3 percentage points regarding inflow velocity and about 0-6 percentage points regarding cell size when turbulence damping is included in the calculation.

The performance of the surface condensation model appears to be promising. It performed extremely well in the case of low flow velocities in the validation geometry. The best results were obtained using 20 mm dimension cells in the computational grid, which is reasonable for practical simulations using realistic containment structures.

Confidentiality	VTT Public

Espoo 9.1.2024

Written by

Jouni Syrjänen,
Senior Scientist

Reviewed by

Timo Niemi,
Senior Scientist

VTT's contact address
VTT Technical Research Centre of Finland Ltd, P.O. Box 1000, FI-02044 VTT, Finland

Distribution (customer and VTT)

SAFER2028 Technical Advisory Group 2.1, Jouni Syrjänen (VTT), Ville Hovi (VTT), Timo Niemi (VTT), Juho Peltola (VTT)

The use of the name of "VTT" in advertising or publishing of a part of this report is only permissible with written authorisation from VTT Technical Research Centre of Finland Ltd.

Approval

VTT TECHNICAL RESEARCH CENTRE OF FINLAND LTD

Date:	9.1.2024
Signature:	
Name:	Antti Arasto
Title:	Vice President, Industrial Energy and Hydrogen

Preface

This work has been done in project CeReSa, where Work Package 1 (WP1) focuses on simulation of hydrogen transport in containment. The CeReSa project is part of the SAFER2028 programme (The Finnish Research Programme on Nuclear Power Plant Safety, 2023–2028). In WP1, simulations of containment building are conducted with ANSYS Fluent (Fortum) and OpenFOAM (VTT). The present report focuses on the OpenFOAM validation simulations of a condensation model developed and implemented at VTT.

This task has been funded by the National Nuclear Waste Management Fund (VYR), VTT Technical Research Centre of Finland Ltd, and Fortum Power and Heat Oy.

Espoo 12.1.2024

Contents

1. Introduction

The containment building of a nuclear power plant houses the reactor core in its pressure vessel and in case of a pressurised water reactor, the primary coolant circuit with its main components such as primary coolant pipes, pumps, steam generators and pressurizer. The purpose of the containment is to prevent the release of radioactive isotopes to the atmosphere in case of a severe accident, where the integrity of the primary coolant circuit has been compromised. It is considered the fourth restraint in the defence of depth strategy to prevent such leaks, following fuel ceramic, fuel cladding tubes, and reactor pressure vessel. Careful design of structural components and safety system ensures that the containment remains intact and can withstand the pressure and heat loads encountered during a severe accident. Containment analysis plays a pivotal role in assessing and enhancing the resilience of these structures and the performance of the safety systems, thereby minimizing the risk of catastrophic incidents and mitigating the consequences of severe accidents.

Most severe accident scenarios are accompanied by a loss of coolant accident, which leads to large amounts of steam getting released into the containment building, and later possibly to a hydrogen release from the overheated fuel. The steam release increases the temperature and pressure in the containment. To decrease its harmful effects, steam is condensed by cooling condensers and on the surfaces of cold containment structures, where the condensate is collected to purpose-built pools or sumps. The hydrogen release in turn may result in stratification and high hydrogen concentrations in parts of the containment, and with oxygen, possibly to combustible or explosive mixtures. Hydrogen risks are reduced by placing several recombiners around the containment building to decrease local hydrogen concentrations by turning hydrogen and oxygen into water vapour in a controlled manner.

Computational Fluid Dynamics (CFD) has emerged as a useful tool in the nuclear safety assessment. It can be used to analyse several safety related issues. 3D distributions of temperature, pressure, and gas composition provided by a CFD simulation can be used, for example, to evaluate the distribution and transport of radioactive isotopes within the containment, to reveal possible risk areas where flammable hydrogen mixtures might occur, and to aid in the design and placement of recombiner systems. Earlier CFD simulations at VTT have been conducted by Huhtanen and co-workers using ANSYS Fluent software (Heitsch et al., 2010). In the current CeReSa project, the aim is to create a containment model for simulations with the OpenFOAM CFD software at VTT. Individual models describing the relevant phenomena are developed, implemented and validated to complete the model with improved usability and reliability.

2. Containment model

Work Package 1 considers CFD modelling of transport of gaseous releases in containment building in case of a major accident, e.g., a prolonged primary circuit coolant pipe leak leading to a severe accident where the reactor core is damaged. In such scenarios, the understanding of the behaviour of the most significant gas components such as hydrogen, oxygen, and steam, which are released during the accident, is highly important in order to ensure the functionality of the containment safety features. 3D CFD modelling provides a useful tool for predicting the local flow conditions in the containment volume.

The most relevant phenomena taking place inside containment buildings during severe accidents were identified in the Phenomena Identification and Ranking Table (PIRT) process, conducted as part of Task 2 of Work Package 1. Submodels for the selected, highly ranked phenomena are (or will be) developed, implemented, and validated by VTT in Task 1 of Work Package 1. Ultimately, all the developed submodels are combined to form an OpenFOAM model that can be used to simulate conditions occurring in nuclear power plant containment buildings during severe accidents. Corresponding simulations are conducted by Fortum using the ANSYS Fluent software in Task 2 of Work Package 1.

Condensation was one of the most essential phenomena identified in the PIRT process. The steam released during severe accidents may condense on containment walls, cooling condensers and ice or pool surfaces. Local flow field, temperature, pressure, and gas composition determine the local condensation rates, but on the other hand, condensation and re-evaporation processes affect the flow patterns, and the distribution of gas components that are formed within the containment. The wall condensation model, presented below in Section 3, can be applied or extended to describe condensation on various surfaces, which were listed in the PIRT process as separate phenomena. Extending the wall condensation model for ice surfaces, creating a model for the ice melting, developing a model for the recombiners, and validation calculations are among the planned future actions in Task 1.

The present investigation, reported here, concerns the validation of the surface condensation model developed and implemented in OpenFOAM CFD software at VTT. The model is based on multicomponent diffusion. A suitable experimental setup with adequate measurement data is selected for model validation. A sensitivity study of computational grid density is also included.

3. Wall condensation model

The molar fluxes of non-condensable gas, J_{gas} [mol/m^{2}s], and steam, J_{H_2O} [mol/m^{2}s], through a plane parallel to the wall at a distance of δ [m] from the wall, are given by the following pair of differential equations:

$$J_{\text{gas}} = Jx_{\text{gas}} - D_{\text{Eff,gas}-H_2O} \cdot c \frac{dx_{\text{gas}}}{dy} = 0 \tag{3.1}$$

$$J_{H_2O} = Jx_{H_2O} - D_{\text{Eff,gas}-H_2O} \cdot c \frac{dx_{H_2O}}{dy} \tag{3.2}$$

where

$D_{\text{Eff,gas}-H_2O}$	effective diffusion coefficient (for steam in a gas mixture) [m^2/s],
J	convective mixture molar flux [mol/m^{2}s],
c	mixture molar concentration [mol/m^3],
x_{gas}	molar fraction of non-condensable gas [-], and
x_{H_2O}	molar fraction of steam [-].

Since there is no net flow of non-condensable gas through the plane, the pair of equations can be reduced to:

$$J_{H_2O} = -D_{\text{Eff,gas}-H_2O} \cdot c \frac{dx_{H_2O}}{dy}\left(\frac{x_{H_2O}}{x_{\text{gas}}} + 1\right) = -D_{\text{Eff,gas}-H_2O} \cdot c \cdot \frac{1}{1 - x_{H_2O}} \cdot \frac{dx_{H_2O}}{dy} \tag{3.3}$$

Integration from the wall surface ($y = 0$) to the edge of the boundary layer ($y = \delta$) gives the following relation for the vapor molar flux:

$$\Leftrightarrow \int_0^{\delta} J_{H_2O}\, dy = \int_0^{\delta} -D_{\text{Eff,gas}-H_2O} \cdot c \cdot \frac{1}{1 - x_{H_2O}} \cdot \frac{dx_{H_2O}}{dy} dy \tag{3.4}$$

$$\Leftrightarrow J_{H_2O} \int_0^{\delta} 1\, dy = -D_{\text{Eff,gas}-H_2O} \cdot c \int_0^{\delta} \frac{1}{1 - x_{H_2O}} dx_{H_2O} = D_{\text{Eff,gas}-H_2O} \cdot c \int_0^{\delta} \frac{-1}{1 - x_{H_2O}} dx_{H_2O} \tag{3.5}$$

$$\Leftrightarrow J_{H_2O}(\delta - 0) = D_{\text{Eff,gas}-H_2O} \cdot c \left(\ln\left|1 - x_{H_2O,\delta}\right| - \ln\left|1 - x_{H_2O,0}\right|\right) \tag{3.6}$$

$$\Leftrightarrow J_{H_2O} = \frac{D_{\text{Eff,gas}-H_2O} \cdot c}{\delta} \ln\left(\frac{\left|1 - x_{H_2O,\delta}\right|}{\left|1 - x_{H_2O,0}\right|}\right) \tag{3.7}$$

where $x_{H_2O,0}$ and $x_{H_2O,\delta}$ are steam molar fractions at the wall surface and the edge of the boundary layer, respectively. Steam molar flux, J_{H_2O} [mol/m^{2}s], can be transformed into a mass flux, j_{H_2O} [kg/m^{2}s], by multiplying (3.7) with the steam molar mass:

$$j_{H_2O} = M_{H_2O} J_{H_2O} = \frac{M_{H_2O} D_{\text{Eff,gas}-H_2O} \cdot c}{\delta} \ln\left(\frac{\left|1 - x_{H_2O,\delta}\right|}{\left|1 - x_{H_2O,0}\right|}\right) \tag{3.8}$$

Using the definition of molar concentration

$$c = \frac{n}{V} = \frac{m}{MV} = \frac{\rho}{M} \tag{3.9}$$

the steam mass flux reduces to

$$j_{H_2O} = \frac{M_{H_2O} D_{\text{Eff,gas}-H_2O} \cdot \rho}{M\delta} \ln\left(\frac{\left|1 - x_{H_2O,\delta}\right|}{\left|1 - x_{H_2O,0}\right|}\right) \tag{3.10}$$

Since the model assumes that condensation is limited only by diffusion, it means that the surface of the condensate film that forms on the wall is assumed to be at a saturated state, i.e. vapor partial pressure (p_{H_2O} [Pa]) is equal to saturation pressure (p_{sat} [Pa]):

$$p_{H_2O} \equiv p_{\text{sat}}(T_{\text{w}}) \tag{3.11}$$

Vapor molar fraction at the film surface can be solved from eq. (3.11):

$$x_{H_2O,0} = \frac{p_{\text{sat}}(T_{\text{w}})}{p} \tag{3.12}$$

The effective diffusion coefficient consists of laminar and turbulent terms:

$$D_{\text{Eff,gas}-H_2O} = D_{\text{gas}-H_2O} + \frac{Pr_t}{Sc_t}\alpha_t \tag{3.13}$$

The multicomponent diffusion coefficient (for steam in a gas mixture) is used for the laminar term and the turbulent term is calculated from the thermal wall function for turbulent thermal diffusion, α_t, with the help of turbulent Prandtl and Schmidt numbers, Pr_t and Sc_t, respectively. Constant values of $Pr_t = 0.85$ and $Sc_t = 0.7$ were selected for the simulations presented here. The Jayatilleke model was selected for the turbulent thermal diffusion wall function.

The multicomponent mass diffusion coefficient for the diffusion of steam in a three-component gas mixture (steam, oxygen, and nitrogen), is calculated as proposed by Fairbanks and Wilke (1950, eq. 3):

$$D_{\text{gas}-H_2O} = \frac{\left(1 - x_{H_2O}\right)}{\frac{x_{N_2}}{D_{N_2-H_2O}} + \frac{x_{O_2}}{D_{O_2-H_2O}}} \tag{3.14}$$

The binary diffusion coefficients between two gas components, D_{A-B} [m^2/s], are estimated from the Fuller, Schettler and Giddings relation (Perry and Green, 1984; p. 3-285, eq. 3-133):

$$D_{N_2-H_2O} = \frac{101325 \cdot 10^{-7}\, T^{1.75} \left(\frac{1}{M_{N_2}} + \frac{1}{M_{H_2O}}\right)^{1/2}}{p\left[(\sum v)_{N_2}^{1/3} + (\sum v)_{H_2O}^{1/3}\right]^2} \tag{3.15}$$

$$D_{O_2-H_2O} = \frac{101325 \cdot 10^{-7}\, T^{1.75} \left(\frac{1}{M_{O_2}} + \frac{1}{M_{H_2O}}\right)^{1/2}}{p\left[(\sum v)_{O_2}^{1/3} + (\sum v)_{H_2O}^{1/3}\right]^2} \tag{3.16}$$

where
M_{H_2O} molecular weight of vapor ($M_{H_2O} = 18.016$) [g/mol],
M_{O_2} molecular weight of oxygen ($M_{O_2} = 31.998$) [g/mol],
M_{N_2} molecular weight of nitrogen ($M_{N_2} = 28.013$) [g/mol],
p absolute pressure [Pa],
T gas temperature [K],
$(\sum v)_{H_2O}$ atomic diffusion volume for vapor ($(\sum v)_{H_2O} = 12.7$) [-],
$(\sum v)_{O_2}$ atomic diffusion volume for oxygen ($(\sum v)_{O_2} = 16.6$) [-] and
$(\sum v)_{N_2}$ atomic diffusion volume for nitrogen ($(\sum v)_{N_2} = 17.9$) [-].

4. Validation calculations

To evaluate the performance of the newly developed surface condensation model, the CONAN test facility, described by Ambrosini et al. (2008), was selected as the validation case.

4.1 Description of the CONAN facility

The CONAN experimental facility is located at the University of Pisa. It was used for benchmark step 1 of SARnet Network of Excellence in assessing the status of the condensation models implemented in the prevailing CFD software intended for modelling nuclear reactor containment applications.

The test section of the CONAN facility, depicted in Figure 1, consists of a primary test channel for the gas phase, a cooled plate for condensation as one of its vertical sides, and a secondary coolant channel on the other side of the plate. The primary test channel is 2 m in height and 0.34 m × 0.34 m in horizontal cross section. The cooled side plate is 4.5 cm thick aluminium implying 0.34 m × 0.045 m horizontal cross section. The rear side of the plate is cooled by coolant flowing in the secondary coolant channel with 5 mm depth, and hence 0.34 m × 5 mm horizontal cross section, respectively.

The mixture of steam and air enters the primary test channel from above through honeycomb panels to ensure uniform flow at the inlet. The honeycomb structure consists of three 35 mm thick panels with 3 mm honeycomb cell diameter. Condensation takes place on the surface of the cooled, vertical plate, and the condensate film that is formed flows downwards along the plate. The condensate is collected at the bottom of the plate, where both the mixture of steam and air and the condensate exit the primary test channel. The other three sides of the primary test channel are considered adiabatic. The coolant enters the secondary coolant channel from the bottom. It flows upwards, exiting at the top of the coolant channel.

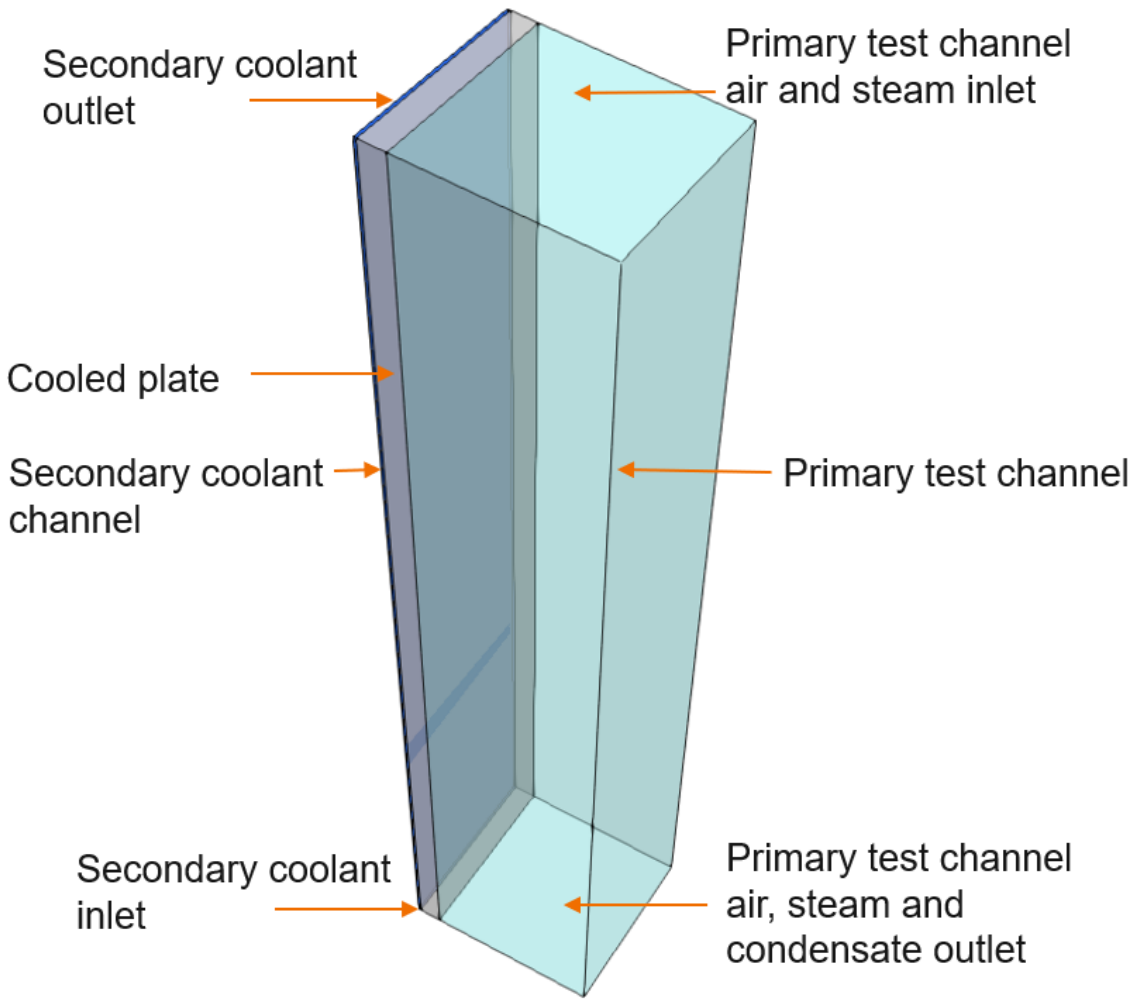

Figure 1. The CONAN test device. The primary test channel for steam and air mixture shown in light blue, the cooled plate shown grey, and the coolant channel shown dark blue.

4.2 Simulated cases

A set of experiments was selected, which varied the inflow velocity of the steam-air mixture. However, due to the experimental setup, the temperature and composition of the gas mixture also varied between the different experiments. The test cases and the corresponding steam flow rates are shown in Table 1.

Table 1. Simulated test cases and the corresponding steam mass inflow values.

Condensation case	Steam inflow (g/s)
P10-T30-V15	54.2
P10-T30-V20	69.0
P10-T30-V25	78.7
P10-T30-V30	82.0
P10-T30-V35	95.9

4.3 Computational grids

To study the effect of mesh resolution, several 2D rectangular computational grids with different cell sizing were created. Square cells were used in the fluid area of the primary test channel. The cases listed in Table 1 were simulated with all of them. The cell dimensions of the computational grids used in the mesh sensitivity study are listed in Table 2. The cell dimension, in Table 2, refers to the length of the side of the square cells in the primary test channel. Examples of computational grids are illustrated in Figure 2, where 34 mm and 5 mm grids are shown.

Table 2. Cell dimensions and the corresponding number of cells for the computational grids used in the simulations.

Cell dimension (mm)	Number of cells
34.0	1475
20.0	3200
10.0	9800
5.00	33200
2.50	120800

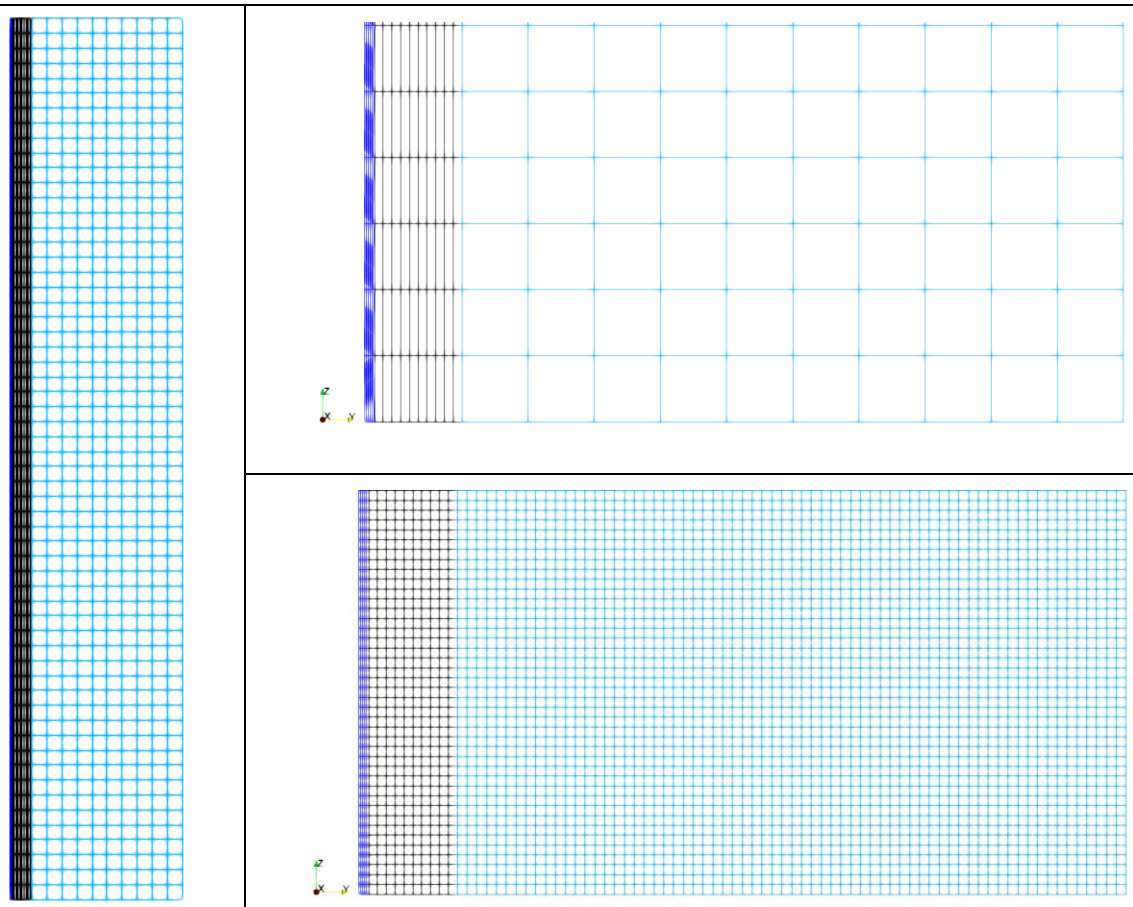

Figure 2. Computational grids used in simulations. All simulations were conducted using 2D rectangular grids. 34 mm cell dimension grid for the whole computational domain (left), detail of it (right, upper), and detail of 5 mm cell dimension grid (right, lower) are shown.

4.4 Modelling approach

In addition to the primary test channel where the mixture of steam and air flows and condensation takes place, the cooled plate and the secondary cooling channel were included in the CFD model. The conjugate heat transfer (CHT) method of OpenFOAM was used in the multi-region simulation. The primary test channel flow was modelled using the Eulerian multiphase model with the mixture of steam and air as the gas phase and the condensed water as the liquid phase. The gas phase consists of three components: water vapour, oxygen and nitrogen. Turbulence is modelled with the k-ω SST model. Heat conduction in the cooled plate and heat transfer through its surfaces facing the primary test channel and the secondary cooling channel are included in the model. Single phase flow and convective heat transfer modelling is applied to the coolant flow in the cooling channel.

The simulations were performed both with and without turbulence damping in the primary test channel. The turbulence damping limits the production of turbulence at free surfaces, such as water pools. Therefore, damping is necessary for realistic containment simulations where complete phase inversion and free surfaces occur. However, for the CONAN experiments, there is no real need for the turbulence damping since phase inversion is not expected.

4.5 Simulation results

Simulations of condensation experiment in CONAN test device were conducted with various mixture of steam and air flow rates and grid densities. The simulation results are presented in Table 3, where the predicted condensation rates are compared with the corresponding experimental values. The comparison is also shown in Figure 4 and Figure 5. The dependency of simulated condensation rates on inflow velocity and grid density are presented in Tables 4 and 5 without turbulence damping, and in Tables 6 and 7 with turbulence damping, respectively.

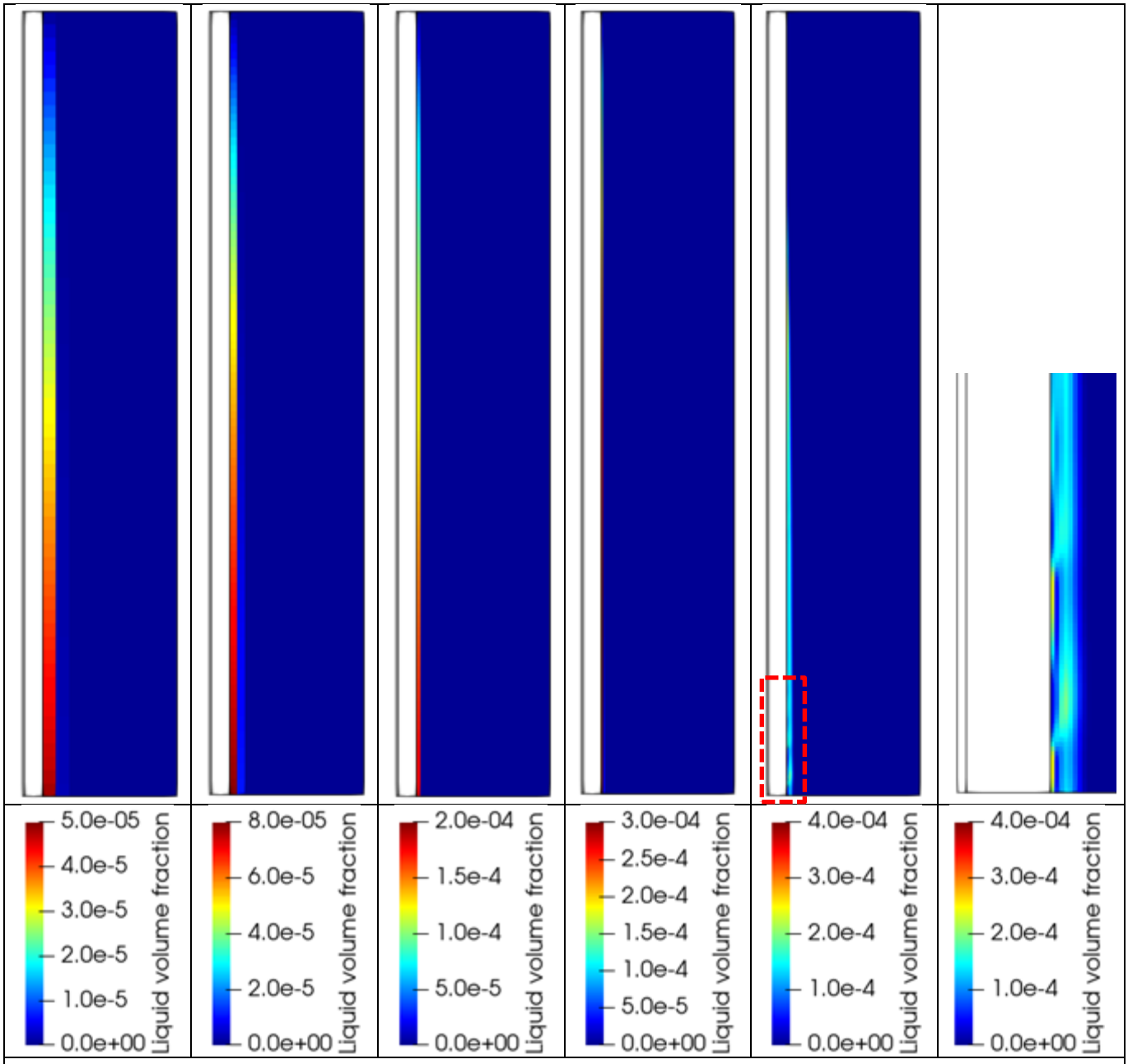

Figure 3. Contours of liquid volume fraction, showing the effect of grid density. Cell dimensions from left to right: 34 mm, 20 mm, 10 mm, 5 mm and 2.5 mm. Far right detail of the 2.5 mm cell grid prediction of the wavy liquid structures separating from the cooled plate.

Table 3. Comparison of measured and simulated condensation rates using various inflow velocities and grid densities with and without turbulence damping.

Condensation case	Condensation rate in experiment (g/s)	Condensation rate in simulation (g/s)		Ratio of calculated and measured values (%)	
		Turbulence damping		Turbulence damping	
		Off	On	Off	On
P10-T30-V15-34.0mm	2.315	2.124	2.122	91.75	91.69
P10-T30-V15-20.0mm	2.315	2.296	2.289	99.18	98.90
P10-T30-V15-10.0mm	2.315	2.315	2.274	100.02	98.26
P10-T30-V15-5.00mm	2.315	2.148	2.043	92.79	88.26
P10-T30-V15-2.50mm	2.315	2.371	2.281	102.44	98.56
P10-T30-V20-34.0mm	2.468	2.291	2.290	92.83	92.78
P10-T30-V20-20.0mm	2.468	2.411	2.402	97.71	97.34
P10-T30-V20-10.0mm	2.468	2.348	2.291	95.14	92.83
P10-T30-V20-5.00mm	2.468	2.230	2.034	90.34	82.40
P10-T30-V20-2.50mm	2.468	2.563	2.396	103.87	97.07
P10-T30-V25-34.0mm	2.601	2.322	2.321	89.27	89.23
P10-T30-V25-20.0mm	2.601	2.411	2.401	92.71	92.32
P10-T30-V25-10.0mm	2.601	2.315	2.232	89.00	85.81
P10-T30-V25-5.00mm	2.601	2.320	2.115	89.21	81.32
P10-T30-V25-2.50mm	2.601	2.441	2.326	93.84	89.43
P10-T30-V30-34.0mm	2.657	2.162	2.162	81.38	81.36
P10-T30-V30-20.0mm	2.657	2.226	2.217	83.79	83.43
P10-T30-V30-10.0mm	2.657	2.136	2.032	80.41	76.49
P10-T30-V30-5.00mm	2.657	2.127	2.014	80.06	75.79
P10-T30-V30-2.50mm	2.657	2.146	2.081	80.79	78.32
P10-T30-V35-34.0mm	2.979	2.366	2.365	79.42	79.41
P10-T30-V35-20.0mm	2.979	2.431	2.421	81.61	81.28
P10-T30-V35-10.0mm	2.979	2.328	2.228	78.14	74.80
P10-T30-V35-5.00mm	2.979	2.315	2.218	77.72	74.45
P10-T30-V35-2.50mm	2.979	2.337	2.280	78.45	76.54

4.5.1 Simulations without turbulence damping

The best average accuracy of simulated condensation rates is achieved in test cases with the lowest velocities. The agreement between simulated and measured condensation rates regarding inflow velocity is excellent in 1.5 m/s test case with average discrepancy below 4%, and very good in 2.0 m/s case with average discrepancy below 6%.

The agreement is still relatively good in the 2.5 m/s case test with the average discrepancy below 10%. However, the predicted average condensation rate is just below the one obtained in 2.0 m/s case, although the corresponding experimental value is higher in the 2.5 m/s case.

The measured condensation rates reach the highest two values in the 3.0 m/s and 3.5 m/s inflow test cases, while the lowest average simulated condensation rate takes place in 3.0 m/s case, and the rate next to the lowest in 3.5 m/s case. The discrepancy to experimental condensation rates increases to around 20% in these simulation cases. Similar behaviour of several CFD simulations was also reported by Ambrosini et al. (2008). The reason for this phenomenon may be lower relative humidity especially in the 3.0 case compared to other cases.

Cell dimension, depending on grid density, has a smaller effect on averaged simulation accuracy, presented in Table 5. Figure 4 also shows the small difference between 20 mm cell dimension results and cell dimension averaged results. Best agreement compared to measured condensation rates was obtained using computational mesh with 20 mm cell dimension, leading to 9% averaged discrepancy with various inflow velocities.

The result achieved with 2.5 mm cell dimension is quite close to 20 mm cell dimension result with less than 11% averaged discrepancy compared to experiments. Calculations with 2.5 mm cell dimension grid overpredict the condensation rates slightly in 1.5 m/s and 2.0 m/s test cases compared to measured rates. All the other simulations underpredict the condensation rates in all test cases without turbulence damping except in 1.5 m/s 10 mm cell dimension case.

The simulations with 2.5 mm cell dimension grid indicate some time dependent behaviour by formation of liquid phase flow structures near the lower part of the cooling plate, as shown in Figure 3, far right. This leads to a short time step size and to a long simulation time, which in turn suggest modelling of the condensation with a liquid film model instead of a Eulerian multiphase model.

It is worth noting that the number of cells is only 3200 in the 20 mm cell dimension grid and almost forty-fold, 120800, in the 2.5 mm cell dimension grid.

Other simulation results with 11, 34 and 5 mm cell dimension grids have discrepancy rates between 11.5% and 14% compared to experimental results.

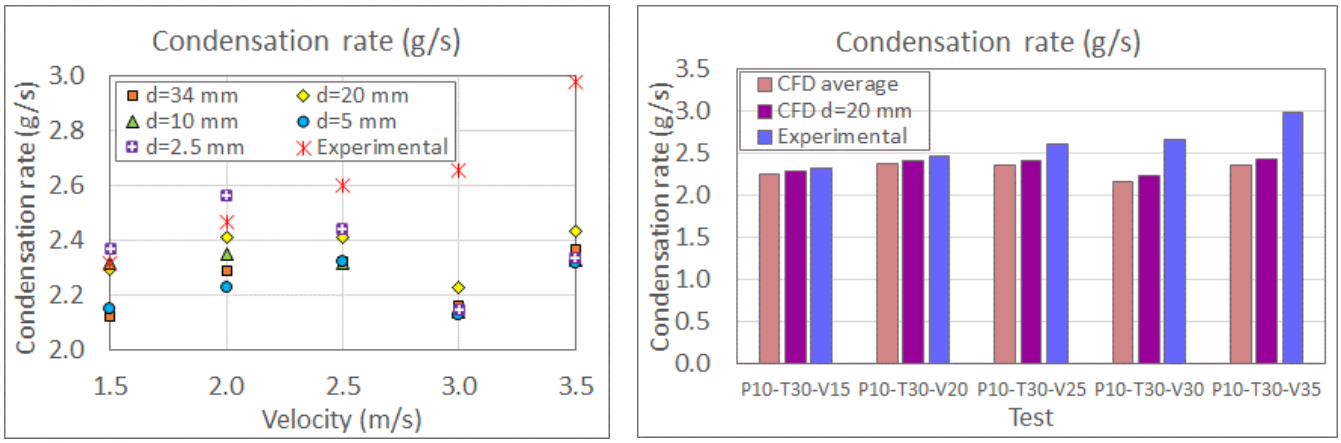

Figure 4. Without turbulence damping simulated and measured condensation rates. Individual (left) as well as cell dimension averaged and best (cell dimension 20 mm) simulation results (right).

Table 4. Cell dimension averaged discrepancy between measured and simulated condensation rates depending on inflow velocity without turbulence damping.

Condensation case	Average discrepancy (%)
P10-T30-V15	3.8
P10-T30-V20	5.6
P10-T30-V25	9.2
P10-T30-V30	18.7
P10-T30-V35	20.9

Table 5. Inflow velocity averaged discrepancy between measured and simulated condensation rates depending on cell dimension without turbulence damping.

Cell size (mm)	Average discrepancy (%)
20.0	9.0
2.50	10.6
10.0	11.5
34.0	13.1
5.00	14.0

4.5.2 Simulations with turbulence damping

Calculations were also conducted with turbulence damping using parameter $\delta=10^{-4}$. The turbulence damping model implemented in OpenFOAM is the model of Frederix et al. (2018) which has been generalized to work with unstructured meshes.

Generally, the predicted condensation rates were lower than without turbulence damping. Individual values range from roughly 0 to 8 percent points less than undamped values. The condensation rates presented in Table 3 are illustrated in Figure 5. Corresponding average discrepancies compared to experimental values are shown in Tables 6 and 7.

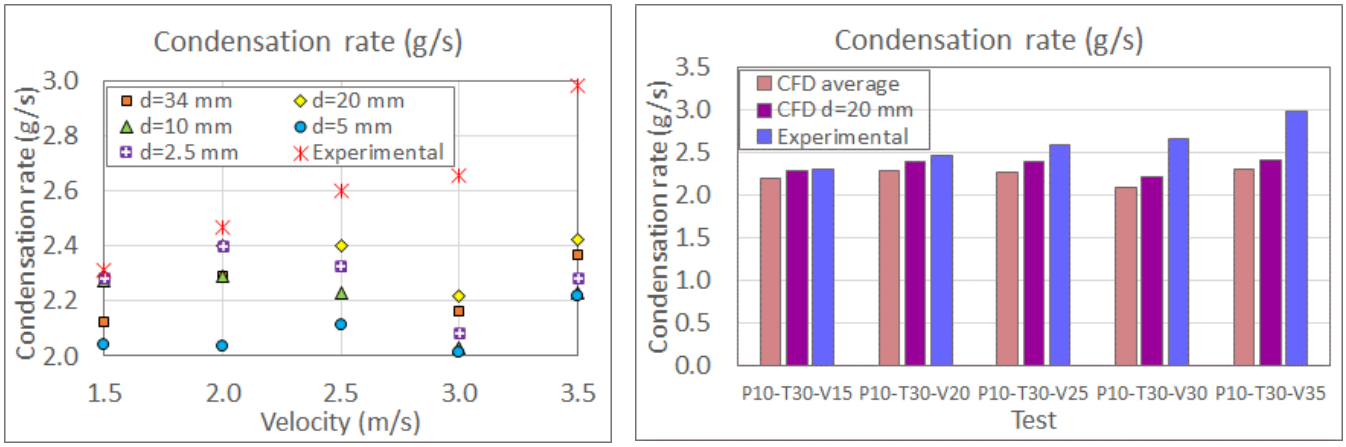

Figure 5. With turbulence damping simulated and measured condensation rates. Individual (left) as well as cell dimension averaged and best (cell dimension 20 mm) simulation results (right).

Regarding inflow velocity, the cell size averaged discrepancy between simulated and measured condensation rates increases by about 1-3 percent points with turbulence damping when compared with simulations without turbulence damping. The averaged agreement is still good in 1.5 and 2.0 m/s cases, and rather good in the 2.5 m/s case, while in the 3.0 and 3.5 m/s cases the averaged discrepancy to measured condensation rates rises above 20%.

Concerning cell size, the inflow velocity averaged discrepancy increases by roughly 0 to 6 percent, resulting in values from about 9% to 20%. Simulations with 20 mm and 2.5 mm cell dimensions provide still the best average agreement with experimental condensation rates. The average discrepancy remains the same with 34 mm cell dimension. Simulation results with 10 mm and 5 mm cell dimension deviate most from measured values. Especially the 5 mm cell dimension average agreement declines when average discrepancy increases from 14% to about 20%.

Table 6. Cell dimension averaged discrepancy between measured and simulated condensation rates depending on inflow velocity with turbulence damping.

Condensation case	Average discrepancy (%)
P10-T30-V15	4.9
P10-T30-V20	7.5
P10-T30-V25	12.4
P10-T30-V30	20.9
P10-T30-V35	22.7

Table 7. Inflow velocity averaged discrepancy between measured and simulated condensation rates depending on cell dimension with turbulence damping.

Cell size (mm)	Average discrepancy (%)
20.0	9.3
2.50	12.0
34.0	13.1
10.0	14.4
5.00	19.6

5. Summary and conclusion

Validation calculations of a surface condensation model, developed and implemented in OpenFOAM CFD software at VTT as a part of a containment model, are conducted. The condensation model is based on multicomponent diffusion approach. The model was validated against experiments conducted with the CONAN test facility. The test device contains a channel with a cooled plate where condensation from mixture of steam and air flowing by takes place.

Effects of grid density, inflow velocity and turbulence damping were studied. Validation simulations using various inflow velocities and grid densities with and without turbulence damping were performed.

The agreement of simulated and measured condensation rates is best at low inflow velocities, with cell size averaged discrepancy to measured values below 4% at 1.5 m/s. The average discrepancy then increases with increasing inflow velocity up to about 21% at 3.5 m/s.

Regarding cell size, the best inflow velocity averaged agreement is obtained with 20 mm cell size with 9% discrepancy to measured value. The average discrepancy grows to 14% with 5 mm cell size, but there is no common trend among inflow velocity averaged cell sizes in this range. 20 mm cell size is reasonable to be used in practical containment simulations.

Including turbulence damping in the modelling decreases the condensation rates to some degree. The average discrepancy between simulated and measured condensation rates increases about 1-3 percentage points regarding inflow velocity and about 0-6 percentage points regarding cell size when turbulence damping is included in the calculation.

The performance of the surface condensation model appears to be promising. It performed extremely well in the case of low flow velocities in the validation geometry. The best results were obtained using 20 mm

dimension cells in the computational grid, which is reasonable for practical simulations using realistic containment structures.

References

Ambrosini, Walter; Bucci, M., Forgione, N., Oriolo, Francesco; Paci, Sandro; Magnaud, Jean-Paul; Studer, E., Reinecke, E., Kelm, Stephan; Jahn, W., Travis, J., Wilkening, H., Heitsch, M., Kljenak, I., Babic, M., Houkema, M., Visser, D.C., Vyskosil, L., Kostka, P. and Huhtanen, R., (2008). Comparison and Analysis of the Condensation Benchmark Results. Proceedings of the Third European Review Meeting on Severe Accident Research (ERMSAR-2008). 23-25. https://publications.vtt.fi/julkaisut/muut/2008/3-2-Condensation-Paper-Final.pdf

Fairbanks, D. F. and Wilke, C. R., 1950. Diffusion Coefficients in Multicomponent Gas Mixtures. *Industrial & Engineering Chemistry* **1950** *42* (3), 471-475. https://doi.org/10.1021/ie50483a022

Frederix, E. M. A., Mathur, A., Dovizio, D., Geurts, B. J. amd Komen, E. M. J. (2018). Reynolds-averaged modeling of turbulence damping near a large-scale interface in two-phase flow. Nuclear engineering and design, 333, 122-130. https://doi.org/10.1016/j.nucengdes.2018.04.010

Heitsch, M., Huhtanen, R., Téchy, Z., Fry, C., Kostka, P., Niemi, J. and Schramm, B., 2010. CFD evaluation of hydrogen risk mitigation measures in a VVER-440/213 containment. *Nuclear Engineering and Design*. Volume 240, Issue 2, 385-396. ISSN 0029-5493. https://doi.org/10.1016/j.nucengdes.2008.07.022.

Perry, R. H., and Green, D., 1984. Perry's Chemical Engineers' Handbook, 6th edition. New York: McGraw-Hill, Inc. ISBN 0-07-049479-7